14th Australasian Fluid Mechanics Conference
Adelaide University, Adelaide, Australia
10-14 December 2001

Structure of Rough Wall Turbulent Boundary Layers at Relatively High Reynolds Number

S. Bisceglia, R. J. Smalley, L. Djenidi and R. A. Antonia

Department of Mechanical Engineering
University of Newcastle, New South Wales, 2308 AUSTRALIA

Abstract

The effect of two different types of surface roughness on a turbulent boundary layer was studied using 2-component LDV measurements in a relatively high speed water tunnel. One roughness consists of square bars at a streamwise spacing p equal to $2k$ (k is the roughness height). The other consists of cylindrical rods with p/k equal to 4. Both roughnesses are aligned in a direction transverse to the flow. Measurements of the turbulent field were carried out over a wide range of Reynolds numbers, ($1\,500 < R_\theta < 23\,000$) based on the momentum thickness. Comparison of the turbulent field between different surfaces is made at $R_\theta \sim 9\,000$. This study supports previous attempts to classify rough surfaces according to their turbulence characteristics, and extends them by providing measurements at high Reynolds numbers for three distinct surface conditions.

Introduction

The structure of the velocity field in a smooth wall boundary layer is relatively well documented [4, 9]. At sufficiently large Reynolds numbers ($R_\theta \equiv U_1\theta/\nu > 5000$, where θ is the momentum thickness and U_1 is the freestream velocity) the near-wall flow is affected by the wall shear stress u_τ and the viscous length scale ν/u_τ.

By contrast, for a fully-rough wall boundary layer, the roughness element geometry and spacing plays a more important role than the viscous length scale in defining the near-wall turbulence structure. It is usually considered that the roughness will directly influence up to approximately 4 roughness element heights from the wall. The flow within this region is defined as the roughness sublayer. However beyond this region, and at sufficiently large R_θ, Perry & Abell [10] suggested that the turbulence structure should become independent of the wall surface condition. This wall similarity is an extention of Townsend's Reynolds number similarity hypothesis [14]. Clauser [2] suggested that a distinction between rough and smooth walls may be represented using a profile of the normalised mean velocity U^+, plotted as a function of the wall-normal distance y^+. In the logarithmic region, a roughness function ΔU^+ accounts for the shift in U^+ between rough and smooth walls,(+ indicates normalisation by inner scales u_τ and ν/u_τ). Perry et al. [11] proposed a method of classifying rough walls based on the effect the roughness has on ΔU^+. These authors suggested that, for one particular roughness type—a transverse square-bar roughness with a roughness element spacing equal to the roughness height (the so-called d-type)—ΔU^+ scales logarithmically with the boundary layer thickness δ^+. This scaling of ΔU^+ for the d-type contrasts with that over other roughness geometries, where ΔU^+ varies logarithmically with the roughness height k^+. Using an extensive set of rough-wall U^+ data (from both atmospheric surface layer and wind-tunnel measurements), Raupach et al. [12] showed that for each distinct wall surface, ΔU^+ has a unique logarithmic scaling with k^+.

A more complete test of wall similarity, however, requires a comparison of the entire turbulent field over different wall surfaces. In relatively high R_θ flows, [1, 6, 13] have shown that the turbulent field beyond the roughness sublayer is significantly affected by the wall-surface condition. This is in contrast with the wall similarity hypothesis. These authors used three geometrically-different fully-rough walls and compared the Reynolds stresses and higher-order moments of the streamwise u and wall-normal v velocity fluctuations over each surface. By selecting an appropriate U_1 for each surface, they maintained a constant value for ΔU^+, i.e. the effect of the roughness on U^+ was the same for each surface.

To provide further evidence for the lack of wall similarity, the velocity field over different wall surfaces is compared at a Reynolds number that is sufficiently high. For this comparison, it can be confidently assumed that the effect of the Reynolds number can be neglected. Measurements are carried out over two different rough walls (comprising transverse square-bar and cylindrical-rod roughness elements, figures 1a. and 1b. respectively) and a smooth wall at $R_\theta \approx 9\,000$. The measurements are made at larger R_θ than previously carried out over similar rough surfaces, e.g. Krogstad & Antonia [6] ($R_\theta = 4\,810$) and Djenidi et al. [3] ($900 < R_\theta < 2\,300$) for the rods and bar roughnesses respectively. Over the cylindrical rods, [6] showed that the turbulent field throughout most of the boundary layer was significantly different to that for a smooth wall. However, for the square bar roughness, flow visualisations (see [3] and references herein) indicate that near-wall structures identifiable with those in smooth wall layers, (e.g. longitudinal streaks) also occur over this roughness. In the present study, the turbulent field will be compared between three wall surfaces, with the aim of identifying the extent to which the roughness influences the turbulence structure in the overlying flow.

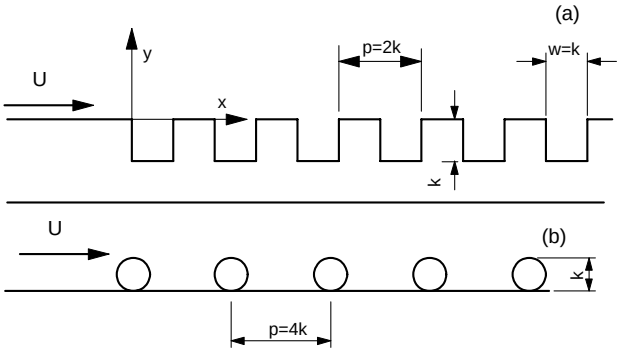

Figure 1: Roughness element geometry and streamwise spacing for the two rough walls. (a). Square bar roughness. $p/k = 2$, $k = 1.9$mm; (b). Cylindrical rod roughness. $p/k = 4$, $k = 3.0$mm.

Experimental Details

The u and v velocity components were measured using two-component laser doppler anemometry (LDA) in a closed-circuit vertical water tunnel. The water temperature was maintained at $17.9 \pm 0.6\,^{o}$C. The boundary layer was tripped using a 30mm long roughness strip (consisting of randomly distributed pebbles and hemispherical elements of diameter ≈ 4.5 mm) which spanned the full width of a 305x155 mm test section made from 20 mm thick perspex. The length of the test section was approximately 1.1 m and the tunnel contraction ratio was 7.95. For each rough wall, two dimensional transverse square-bar and circular-rod roughness elements (height k) were attached to one of the test section walls. These spanned the full width of the test section and were separated at a streamwise pitch p. Figure 1 shows the roughness element geometry and streamwise spacing for the square bar, (a) and cylindrical rod roughness (b). Measurements over the three surfaces were made at 706 mm from the trip, midway between consecutive roughness elements. At this location, a slightly local adverse pressure gradient existed. The free-stream velocity ranged from 0.5 to 4.0 ms^{-1} and the corresponding R_θ varied between 1 500 and 11 000 for the square bar roughness and 2 500 and 23 000 for the cylindrical rods. The LDA fibre optic system, (4W Ar Dantec) consists of one probe used in forward scatter mode. The beam wavelengths used to measure the u and v velocity components were 488μm and 514.5μm respectively and an optical filter was applied to the photomultiplier to reduce noise. The measuring volume dimensions were $l_x = l_y = 0.04$mm and $l_z = 0.63$mm. No seeding was required since the natural impurities in the water were sufficient to obtain a data rate that ranged between 0.1 kHz near the wall, and 4 kHz in the freestream. At each measurement point, 5x10^4 samples were acquired in coincidence mode. The signal processors were two Burst Spectrum Analyzers (57N20-1 BSA Enhanced). The effect of velocity bias was corrected by weighting individual velocity distributions with the transit time of the particles in the measuring volume. To avoid noise, a quality factor was also used. The quality factor is the ratio between the envelope and the pedestal of the LDA signal. Velocity profiles were measured using a 2-direction Dantec lightweight traverse system.

Results

The flow and surface characteristics over the two rough walls and the smooth wall are shown in Table 1. An initial estimate for u_τ was obtained from the maximum in $-\langle uv \rangle$. Assuming that U^+ scales logarithmically with y^+ and also contains an outer-layer wake component, then

$$U^+ = \frac{1}{\kappa}\ln(y+\varepsilon)^+ + C - \Delta U^+ + \frac{2\Pi}{\kappa}\omega(y/\delta) \quad (1)$$

where κ and C are 0.41 and 5 respectively. Here, ε is an empirical error in origin and Π is the wake strength parameter for the wake function ω. For a smooth wall, ΔU^+ and ε are zero. U^+ data fitted to this equation are optimised using the method described in Krogstad et al. [7]. Since the flow is under-developed in the smooth wall layer, Π is less than the nominal value of 0.55. The presence of the roughness enhances the development of the boundary-layer, which increases Π over these surfaces. We estimate that for these surfaces u_τ is determined to an accuracy of approximately 10%. In Figure 2, ΔU^+ for the rod roughness over a range of R_θ is compared with data over the same surface, (also with $p/k = 4$) of

Surface	R_θ	C_fx10^3	ΔU^+	k^+	Π
smooth	8 300	3.10	0	0	0.10
square bar	9 300	3.84	4.1	230	0.35
cylinder rods	9 400	9.08	13.5	400	0.55

Table 1: Flow and surface characteristics for the three surfaces. $C_f \equiv 2{u_\tau}^2/U_1^2$

Krogstad & Antonia [6] and Furuya et al. [5]. All data are in good agreement with

$$\Delta U^+ = \frac{1}{\kappa}\ln k^+ + A. \quad (2)$$

For each surface, different values for the additive con-

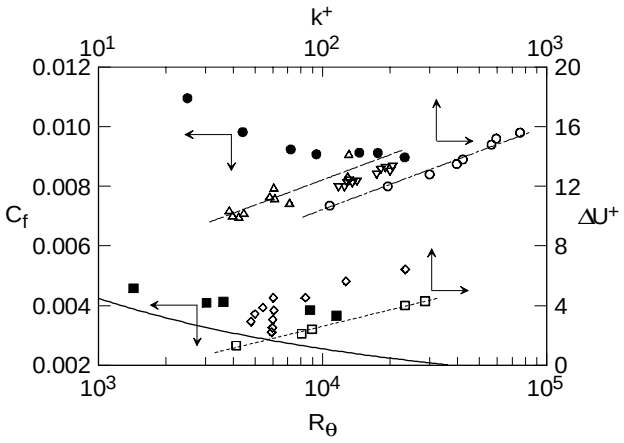

Figure 2: Right and top axes, open symbols. The variation of ΔU^+ with k^+. Circles and triangles, circular rod roughness, $p/k = 4$. ○, present data, - — - curve fit with $A = -0.79$; △,data of [6], — — curve fit with $A = 1.2$; ▽, data of [5]; □ square bar, – – curve fit with $A = -4.74$. ◊, data of [15].
Left and bottom axes, closed symbols. The variation of C_f with R_θ. ●; cylindrical rod roughness. ■ square bar roughness. — Smooth wall data of [4, 9].

stant A indicate a dependence of ΔU^+ on the flow initial conditions (e.g. pressure gradient, trip device, tunnel contraction ratio). While for the square bar roughness, ΔU^+ varies logarithmically with k^+, its slope ($1/\kappa = 0.63^{-1}$) is not equal to the expected value (0.41^{-1}) found for most rough surfaces [12]. This agrees with similar results obtained by Wood & Antonia [15] and suggest that the scaling of ΔU^+ with k^+ cannot be anomalous, nor can it be a consequence of insufficient Reynolds number. There is now sufficient evidence to suggest that ΔU^+ can vary as a function k^+, albeit with a different slope. This contrasts with the classification scheme derived by Perry et al. [11], which requires that ΔU^+ be independent of k^+. We suggest that in (2), a slope equal to 0.41^{-1} is the asymptotic limit for a rough-wall boundary layer. A slope less than 0.41^{-1} is an indication that the boundary layer over a particular wall surface shares characteristics associated with flow over both rough and smooth walls. This conclusion may be applicable to the square bar roughness where $1/\kappa \sim 0.64^{-1}$

The wall skin friction, $C_f \equiv 2[u_\tau/U_1]^2$, is also shown in figure 2 as a function of R_θ. For the cylindrical rod roughness, C_f is approximately independent of Reynolds number when $R_\theta > 10^4$. There is however, insufficient data

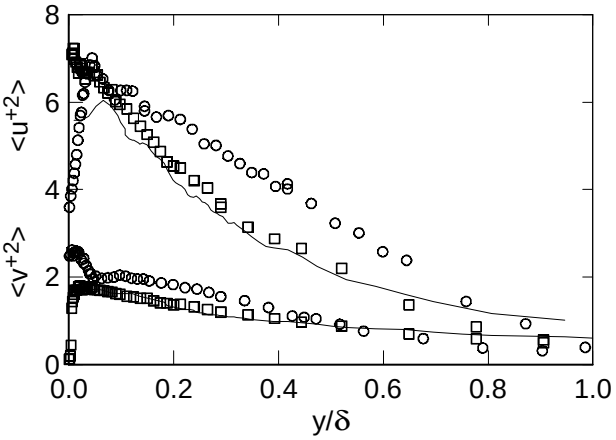

Figure 3: The Normalised Reynolds stresses $\langle u^{+2} \rangle$ and $\langle v^{+2} \rangle$ over three wall surfaces. ○, circular rod; □, square bar; — smooth wall.

over a wide range of R_θ to suggest that C_f for the square bar roughness will also be independent of Reynolds number. The data of [4, 9] show that over a smooth wall, C_f will always decrease with increasing R_θ.

The Reynolds stresses $\langle u^{+2} \rangle$, $\langle v^{+2} \rangle$ and $\langle u^+ v^+ \rangle$ are shown in figures 3 and 4. There are significant differences in the Reynolds stresses between different surfaces within the roughness sublayer. In the outer layer, the most pronounced difference is for the cylindrical rod roughness compared with the smooth wall. The increase in $\langle v^{+2} \rangle$ over the rod-roughness is $\sim 40\%$, compared with a 35% increase in $\langle u^{+2} \rangle$ at $y/\delta = 0.2$. For the square bar however, the intensities are only marginally increased in the outer layer. These characteristics reflect the difference in the roughness element spacing for each surface. By comparison with a smooth wall, the change in the wall surface condition is less severe for the square bar roughness with $p/k = 2$ than with the cylindrical rod roughness ($p/k = 4$). This also agrees with the measurements and flow visualisation of Furuya et al. [5] over circular rods and Liu et al. [8] over square bars. These authors, using a wide range of roughness element spacings showed that, over each wall surface, the flow is more disturbed for $p/k = 4$ than for $p/k = 2$, with an enhancement of mixing around the roughness elements when $p/k = 4$.

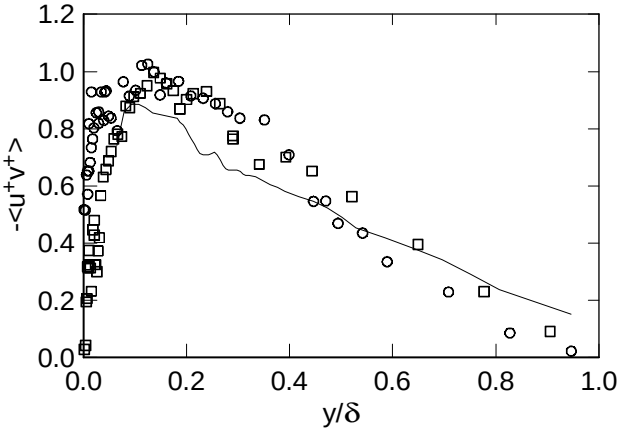

Figure 4: $\langle u^+ v^+ \rangle$ over three wall surfaces. ○, cylindrical rod; □, square bar; — smooth wall.

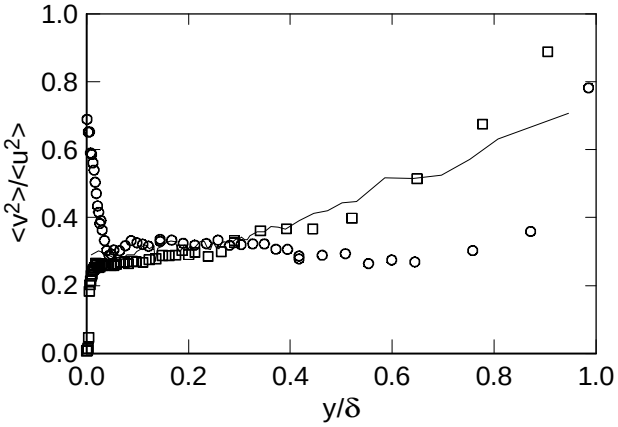

Figure 5: The ratio $\langle v^2 \rangle / \langle u^2 \rangle$ over three wall surfaces. ○, cylindrical rod; □, square bar; — smooth wall.

There is less difference in $-\langle u^+ v^+ \rangle$ (figure 4), between the rough wall surfaces. This contrasts with that observed by [1, 6, 7]. However, over both rough walls, $-\langle u^+ v^+ \rangle$ is increased with reference to the smooth wall. The differences in the Reynolds stresses between all wall surfaces is also apparent when the ratio $\langle v^2 \rangle / \langle u^2 \rangle$ is compared (figure 5). The differences are larger in the near-wall region, with a significantly reduced magnitude of $\langle v^2 \rangle / \langle u^2 \rangle$ over the cavity of a square bar roughness. This may be attributed to the nature of the flow over this surface. Maintained flow recirculation within the cavity decreases the v fluctuations relative to those of u. This is also supported by the visualisations of [3] which show that, apart from intermittent periods of fluid exchange between the cavity the overlying flow, the skimming flow past the cavities is essentially independent of the cavity recirculation.

The skewness ($S_\alpha \equiv \langle \alpha^3 \rangle / \langle \alpha^2 \rangle^{3/2}$) and flatness ($F_\alpha \equiv \langle \alpha^4 \rangle / \langle \alpha^2 \rangle^2$) factors are shown in figures 6 and 7 respectively for $\alpha \equiv u$ and v. While for all surfaces S_u is positive in the near-wall region and crosses zero in the outer layer, over the cylindrical rod roughness the sign-change occurs at larger y/δ. In addition, the distribution of S_v in the near-wall region is negative for the cylindrical rod roughness. These two results imply that strong sweeps, $(u > 0, v < 0)$ are the dominant events that contribute to the near wall flow structure over the rod roughness.

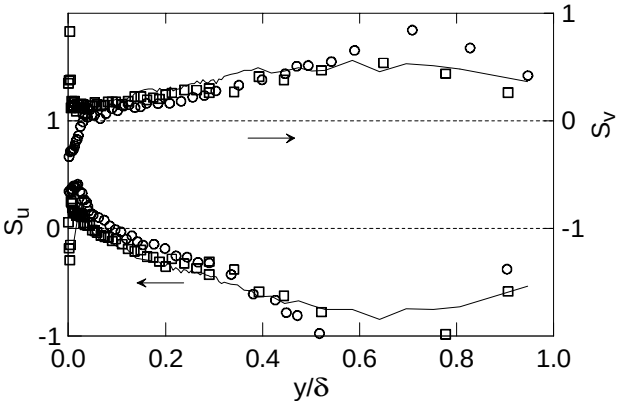

Figure 6: Skewness of u (left axis) and v (right axis) over three wall surfaces. ○, cylindrical rod; □, square bar; — smooth wall.

The quadrant analysis of $-\langle u^+v^+\rangle$, as carried out by [6] and [7] over different wall surfaces, supports this implication. These authors showed that over the rough walls and in particular, the cylindrical rod-roughness, sweeps are stronger than over a smooth wall. In the outer layer and for $y/\delta < 0.5$, there is a systematic variation of both S_u and S_v with roughness geometry. For a smooth wall, the magnitude of both quantities is larger than that for the square bar roughness. S_u and S_v are closest to zero over the cylindrical rod-roughness. The quantities F_u and F_v are used to provide an indication of the large-scale intermittency. Near the wall, the large values of F_v

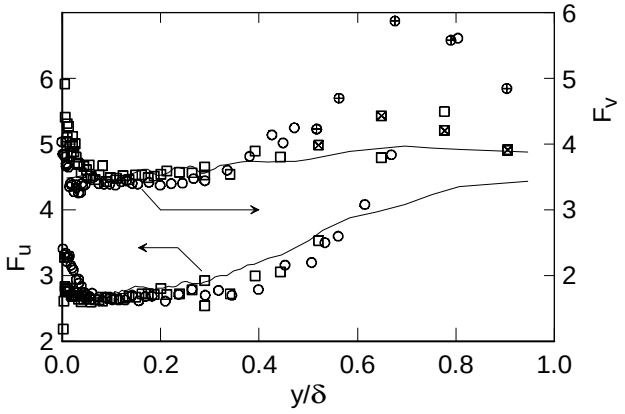

Figure 7: Flatness of u (left axis) and v (right axis) over three wall surfaces. To distinguish between data for $y/\delta > 0.5$, the symbols for F_v are flagged using crosses. ○, cylindrical rod; □, square bar; —, smooth wall.

for the square bar roughness suggest that intense v fluctuations may be associated with the intermittent ejections of fluid away from the cavity into the overlying flow. For the rod-roughness, the results are consistent with intense sweep events which were identified using S_u and S_v. For $y/\delta > 0.6$, the effect of wall roughness increases the magnitude of the skewness and flatness factors for both the u and v fluctuations. Each quantity is larger over the cylindrical rods, compared with both the square bar or the smooth wall, indicating that the influence of the rough wall extends well into the outer boundary layer. Similar conclusions over the rod-roughness at lower Reynolds number were also made by Antonia & Krogstad [1].

Conclusions

LDV measurements carried out in the turbulent boundary layer at large R_θ over two rough walls and a smooth wall show that the turbulent field throughout most of the boundary layer differs between three wall surfaces. The magnitude of R_θ is sufficiently large to assume that Reynolds number effects are not significant. For both rough surfaces, ΔU^+ scales logarithmically with k^+. Over a cylindrical rod roughness (with $p/k = 4$) the mean velocity parameters Π and ΔU^+ are considerably greater than those for the square bar roughness ($p/k = 2$), which are in-turn, larger than those for the smooth wall. The Reynolds stresses $\langle u^{+2}\rangle$ and $\langle v^{+2}\rangle$ are also larger for the cylindrical rod roughness than the smooth wall and square bar roughness. This supports the notion provided by [1] and [6], that the effect of the wall surface extends well beyond the roughness sublayer and provides further support that the wall-similarity hypothesis is not valid for rough wall layers. The skewness and flatness factors indicate that the near-wall structure over the cylindrical rod roughness is dominated by sweep events. In the outer-layer, a systematic dependence of the roughness on the skewness and flatness is apparent.

Acknowledgements

The support of the Australian Research Council (in particular an IREX grant which supports a programme of collaboration with "La Sapienza" University, Roma) and AINSE is gratefully acknowledged. The authors wish to thank D. Wassink for his assistance with the experiment.

References

[1] Antonia, R. A. and Krogstad, P.-Å., Turbulence structure in boundary layers over different types of surface roughness, *Fluid Dyn. Res.*, **28**, 2001, 139.

[2] Clauser, F. H., Turbulent boundary layers in adverse pressure gradients, *J. Aeron. Sci.*, 91–108. Clauser, F. H., The turbulent boundary layer, *Adv. Appl. Mech.*, **4**, 1956, 1–51.

[3] Djenidi, L., Elavarasan, R. and Antonia, R. A., The turbulent boundary layer over transverse square cavities, *J. Fluid Mech.*, **395**, 1999, 271–294.

[4] Fernholz, H. H. and Finley, F. J., The incompressible zero-pressure-gradient turbulent boundary layer: An assessment of the data, *Prog. Aerospace Sci.*, **32**, 1996, 245–311.

[5] Furuya, Y., Miyata, M. and Fujita, H., Turbulent boundary layer and flow resisitance on plates roughened by wires, *J. Fluids Eng.*, **98**, 1976, 635–644.

[6] Krogstad, P.-Å. and Antonia, R. A., Effect of surface conditions on a turbulent boundary layer, *Expt. Fluids*, **27**, 1999, 450–460.

[7] Krogstad, P. Å., Antonia, R. A. and Browne, L. W. B., Comparison between rough- and smooth-wall turbulent boundary layers, *J. Fluid Mech.*, **245**, 1992, 599–617.

[8] Liu, C. K., Kline, S. J. and Johnston, J., An experimental study of turbulent boundary layer on rough walls, Technical Report MD-15, Department of Mechanical Engineering and Stanford University, 1966.

[9] Osaka, H., Kameda, T. and Mochizuki, S., Re-examination of the Reynolds-number-effect on the mean flow quantities in a smooth wall turbulent boundary layer, *JSME Int. J. B.*, **41**, 1998, 123.

[10] Perry, A. E. and Abell, C. J., Asymptotic similarity of turbulence structures in smooth- and rough-walled pipes, *J. Fluid Mech.*, **79**, 1977, 785–799.

[11] Perry, A. E., Schofield, W. H. and Joubert, P. N., Rough wall turbulent boundary layers, *J. Fluid Mech.*, **37**, 1969, 383–413.

[12] Raupach, M. R., Antonia, R. A. and Rajagopalan, S., Rough-wall turbulent boundary layers, *Appl. Mech. Rev.*, **44**, 1991, 1–25.

[13] Smalley, R. J., Krogstad, P.-Å. and Antonia, R. A., Turbulent transport of the Reynolds stresses in a rod-roughened boundary layer, in 13$^{\text{th}}$ *Australasian Fluid Mechanics Conference*, 1998, 615–618.

[14] Townsend, A. A., *Structure of Turbulent Shear Flows*, Cambridge University Press, 1976.

[15] Wood, D. H. and Antonia, R. A., Measurements in a turbulent boundary layer over a d-type surface roughness, *J. Appl. Mech.*, **42**, 1975, 591–597.